Supporting Information for:

Generalized Model for Inhibitor-Modulated 2D Polymer Growth to Understand the Controlled Synthesis of Covalent Organic Frameworks

Shubhani Paliwal,[1,2,$] Wei Li,[3,4,$] Pingwei Liu,[3,4] and Ananth Govind Rajan[1*]*

[1]Department of Chemical Engineering, Indian Institute of Science, Bengaluru, Karnataka 560012, India

[2]Department of Chemical Engineering, Imperial College London, South Kensington Campus, London SW7 2AZ, United Kingdom

[3]State Key Lab of Chemical Engineering, College of Chemical and Biological Engineering, Zhejiang University, Hangzhou 310027, China

[4]Institute of Zhejiang University – Quzhou, 78 Jiuhua Boulevard North, Quzhou 324000, China

***Corresponding Authors:**
Pingwei Liu (E-mail: liupingwei@zju.edu.cn)
Ananth Govind Rajan (E-mail: ananthgr@iisc.ac.in)

[$]S.P. and W.L. contributed equally to this work.

Table of Contents

S1. Effects of Different Additives on COF Synthesis

We found that water did not affect the yield of COF growth, as seen by the comparison of the empty squares and the inverted triangles in Figure S1. Further, we confirmed that the inhibitors used in this work (aniline and benzaldehyde) and their condensation product N-benzylideneaniline had the same effect at a concentration of 12C, as seen by comparing the plus symbols and the upright triangles in Figure S1. This implies that the transformation of the inhibitors into their condensation product provides another inhibition pathway, and indicates the need to include imine exchange reactions in the model in the future.

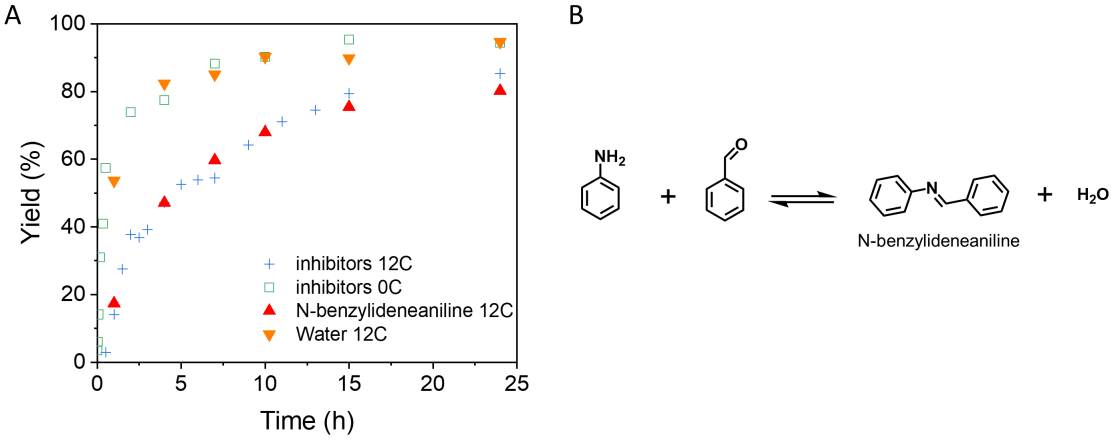

Figure S1. (a) Effects of different additives on COF synthesis. (b) The reaction involved in the formation of N-benzylideneaniline.

S2. Turbidity Measurements of the COF Reaction Mixture

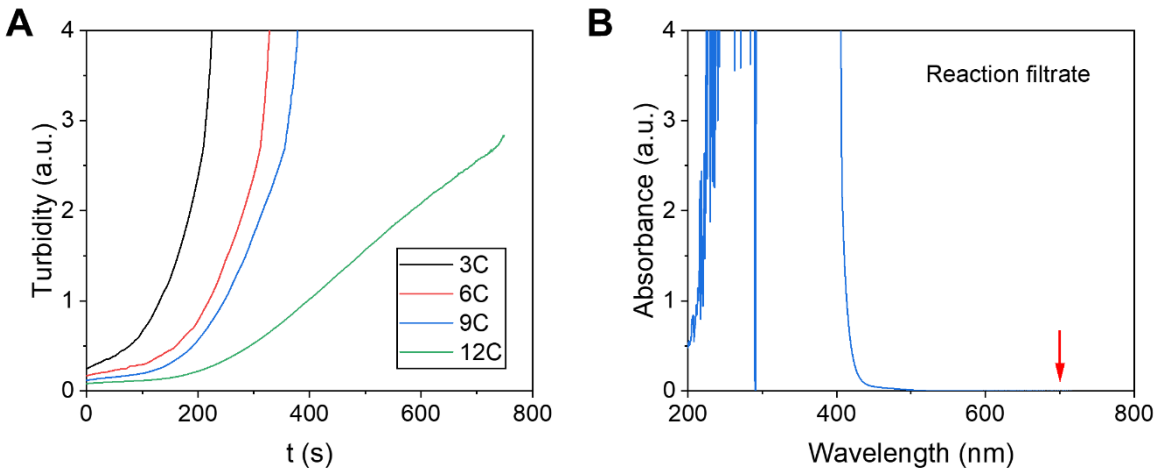

Figure S2. (a) Turbidity of the reaction solutions at 700 nm wavelength as a function of time under 3C, 6C, 9C, and 12C conditions, reflecting the slowing down of the reaction rate with the addition of inhibitors. (b) The absorbance of the filtrate of the reaction solution, showing no interference at 700 nm for turbidity measurements.

S3. Refitted Model for *I*/*M* Ratios Higher than 12 and Its Implications

Note that the kinetic model presented in the main text is trained using the experimental data for the 3C-12C cases, and thus, this set of rate constants obtained cannot be used to predict the COF growth yield as the inhibitor to monomer ratio (*I*/*M*) is further increased beyond 12. A plot of the total yield at 24 h versus the *I*/*M* ratio shows a sharp reduction in yield at *I*/*M* = 12, indicating that it lies at the junction of two differently sloped lines, as seen in our previous work (*Matter* **2019**, 1(6), 1592–1605). This indicates that the mechanism of COF growth inhibition changes when one uses *I*/*M* > 12. To check whether the proposed kinetic model can capture this different mechanism of growth inhibition, we refitted the kinetic model by optimizing the set of rate constants to fit the 15-24C data as shown in Figure S3. Since *I*/*M* = 12 is the point at which the inhibitory mechanism changes, we considered two cases: the first wherein the 12-24C yield data is fit together and the second where the 15-24C yield data are considered together. In either case, we were not able to obtain as good a fit as seen in the main text for the 3-12C cases, indicating that a different model with certain other assumptions may be needed to describe very high inhibitor concentrations. Nevertheless, the fit was better in the latter case considering the 15-24C data with a root-mean square deviation lower than the main text. In this latter case, as seen in Table S1, the values of the rate constants k_m and k_{mr} were close to each other, indicating that k_{mr} likely became high to indirectly account for imine exchange, which is not considered in our model. This is because the condensation product I_{12} can also inhibit COF growth via imine exchange and could be formed in appreciable quantities in the presence of such high concentrations of I_1 and I_2, due to the high rate constant k_i obtained in all cases (even in the main text for the 0-12C cases).

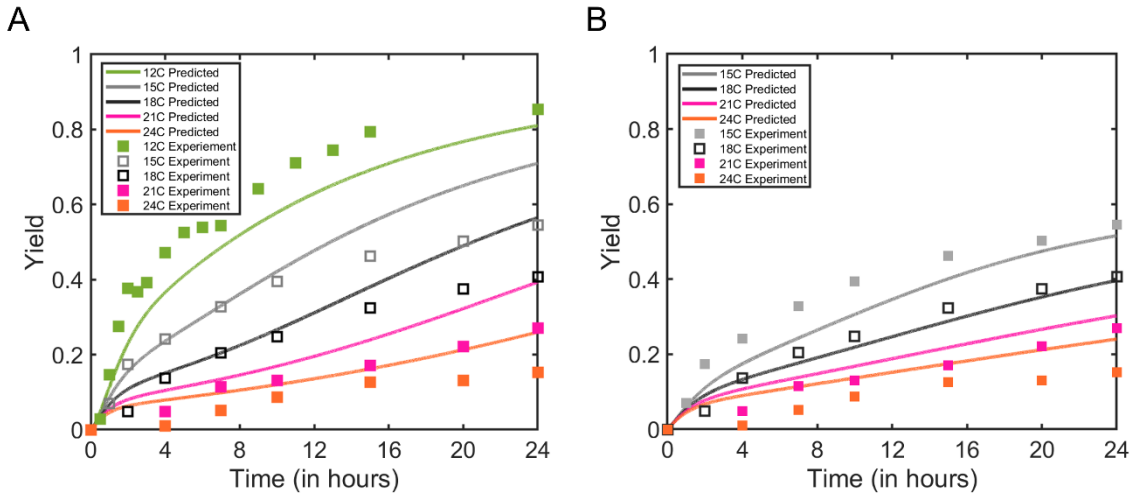

Figure S3. (A) Refitted model 1 considering the 12-24C experimental data and (B) refitted model 2 considering the 15-24C experimental data. Note that the yield is dimensionless.

Table S1. Forward and backward rate constants and enhancement/de-enhancement factors obtained from the data refitting using the mechanistic model. The root-mean-square deviation (RMSD) value between the model predictions and the experimental yield is also indicated.

Refitted Model	RMSD	k_m ($\mathbf{hr^{-1}}$)	k_{mr} ($\mathbf{hr^{-1}}$)	k_i($\mathbf{hr^{-1}}$)	k_{ir} ($\mathbf{hr^{-1}}$)	F_f	F_b
1	0.19	8.2719	0.0038	90.135	0.6633	1169.1	179.43
2	0.06	9.3861	7.2004	72.316	0.6440	3772.5	133.86

S4. Sensitivity Analysis for the KMC Simulation Parameters

We ran KMC simulations with several sets of k_m and k_{ir} values to understand the sensitivity of the model to these parameters. Note that, as explained in the main text, only these two parameters were scaled to get the yield vs. time plots from the KMC simulations to agree with the experimental data. The various sets of rate constant values used are presented in Table S2. The first set of rate constants correspond to the values that gave the best agreement with experiment. These values are slightly tweaked, and 4 sets of rate constants were generated to conduct the sensitivity analysis.

Table S2. Rate constant k_m and k_{ir} values for different test runs chosen for the sensitivity analysis. The multiplicative factors act on the rate constant values (k_{m0} and k_{ir0}) obtained from the theoretical model presented in the main text.

	k_m	k_{ir}	RMSD
Final set	$\mathbf{20k_{m0}}$	$\mathbf{0.03k_{ir0}}$	**0.0699**
1	$20k_{m0}$	$0.02k_{ir0}$	0.0735
2	$20k_{m0}$	$0.04k_{ir0}$	0.0815
3	$15k_{m0}$	$0.03k_{ir0}$	0.0813
4	$25k_{m0}$	$0.03k_{ir0}$	0.0901

The yield plots for all the test runs are presented in Figure S4. As seen in Table S2, in the first two test runs, the rate constant k_m value is kept the same, and k_{ir} is varied. Specifically, in test run 1, the k_{ir} value is decreased and in test run 2, the k_{ir} value is increased. One can see in Figure S4A that a reduction in the k_{ir} value leads to the growth becoming slower, leading to disagreement with the experimental yield vs. time data for the 3C and 6C cases. On the other hand, when the k_{ir} value is increased, as in Figure S4B, the yield increases faster with time, leading to a deviation of the predicted yield vs. time curve for the 12C case from the experimental data.

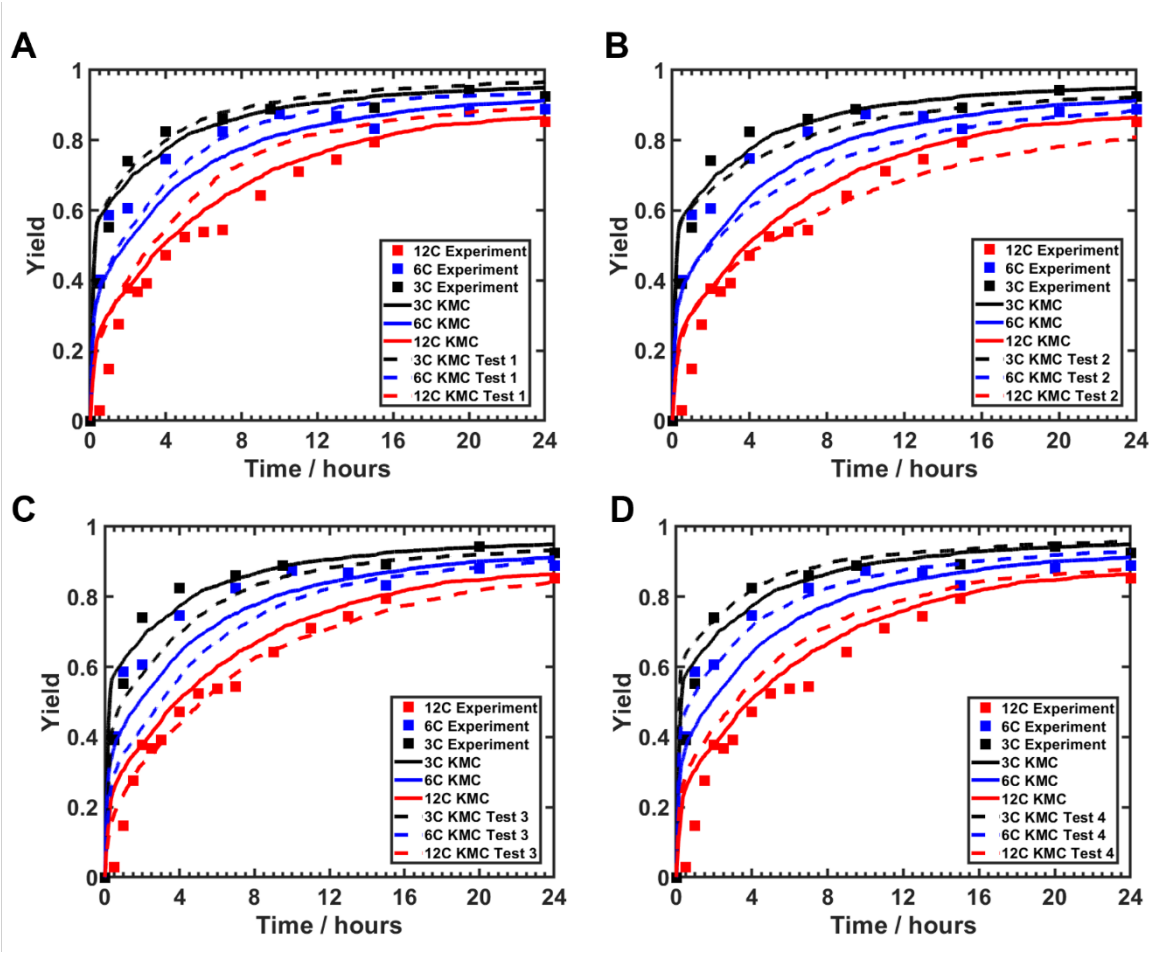

Figure S4. Yield vs. time plots for 4 test runs conducted as a part of the sensitivity analysis of the rate constants k_m and k_{ir}. The dashed lines present the test runs with KMC, the solid lines present the KMC simulation curves with the final set of rate constants, and the symbols represent the experimental yield data. Note that the yield is dimensionless.

For the KMC test runs 3 and 4, the k_{ir} value is kept the same and k_m is varied. Specifically, in test run 3, the k_m value is decreased and in test run 4, the k_m value is increased. Test run 3 (Figure S4C) shows an excellent prediction for the 12C case, but an underestimation of the 3C and 6C yield curves as compared to experiment. This is because the growth becomes slower with time as the k_m value is decreased. Further, the results for test run 4 indicate a good agreement between the 3C and 6C case predictions and the experimental data but an overestimation for the 12C case, due to a speeding up of the growth process. Overall, the parameters chosen in the main text offer the lowest RMSD among the different cases presented, as well as a good match between the experimental data and simulation predictions for the 3C, 6C, and 12C cases.

S5. KMC Simulations Snapshots Until 24 h

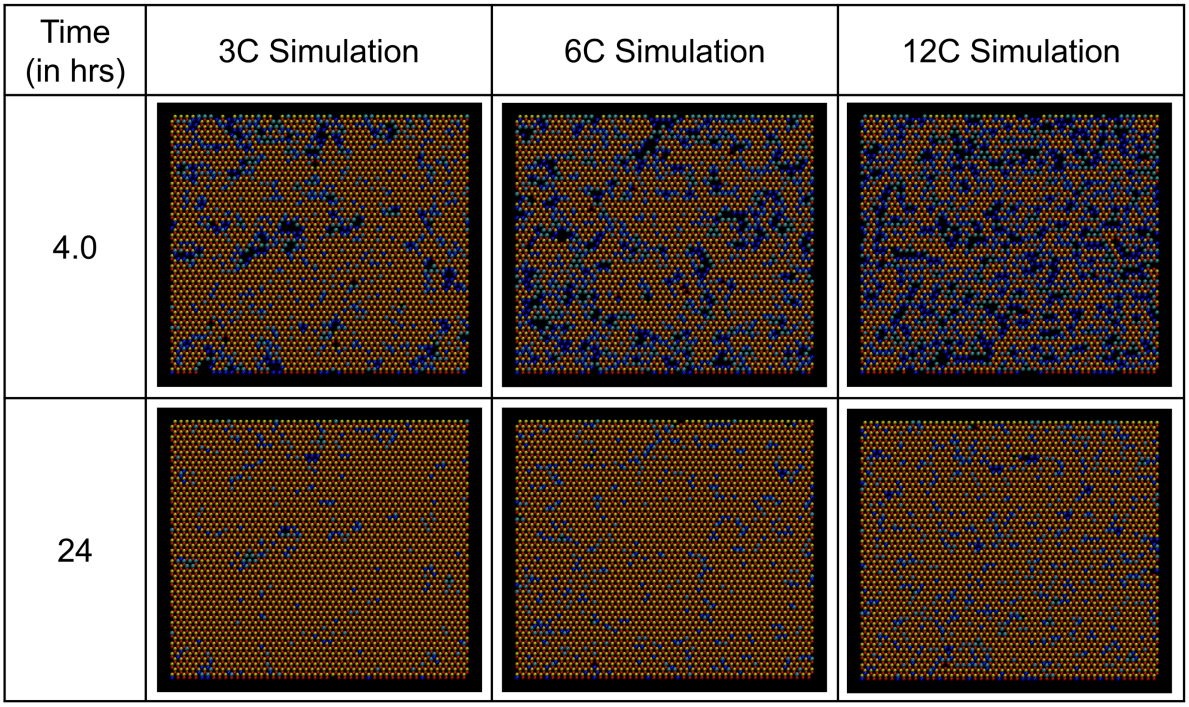

Figure S5. Snapshots from the KMC simulations of COF growth for the 3C, 6C and 12C cases at 4 and 24 hours.

S6. Simulated Flake Size Distribution at 0.13 h

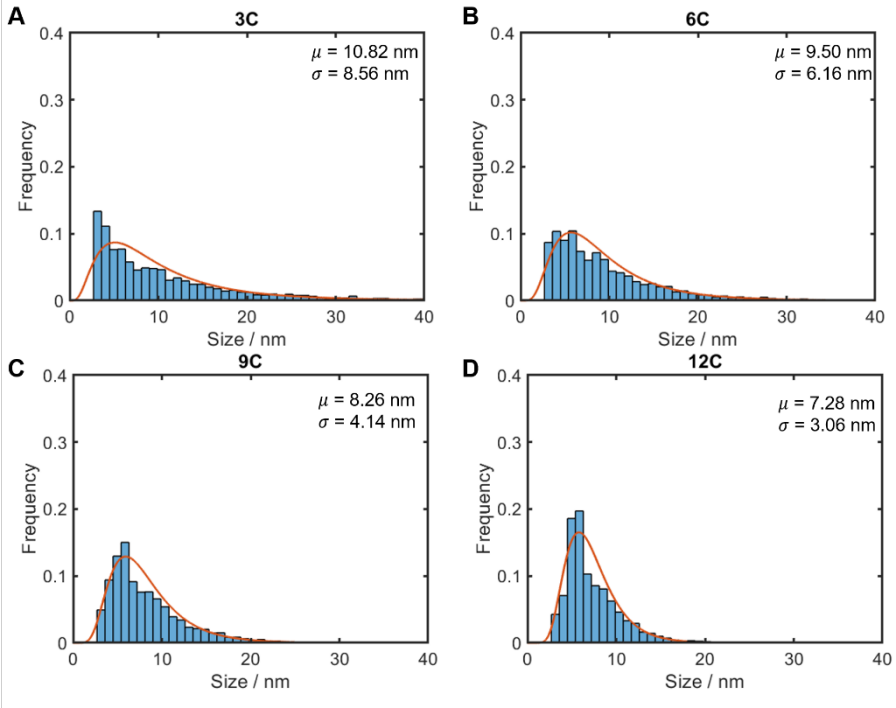

Figure S6. The flake size distribution at 0.13 h of reaction time obtained by averaging the results of 100 KMC simulation runs for different concentrations of inhibitors in the reaction system.

S7. Dynamic Light Scattering (DLS) Measurements

The DLS results verified, in addition to the SEM-based particle size distribution presented in the main text, that the COF flake size decreased with an increase in concentration of the competitors. Note that there is approximately a factor of two difference in the absolute values of the particle size obtained by the two measurement techniques (SEM and DLS), which could be attributed to the swelling and dispersion of particles in ethanol.

Table S3. The particle sizes of the samples obtained using DLS for different amounts of competitors.

Sample	Peak of the particle size distribution (nm)			
	#1	#2	#3	Average
3C at 0.06 h	566	581	616	588
6C at 0.06 h	457	523	577	519
9C at 0.06 h	306	368	397	357
12C at 0.06 h	285	318	386	330

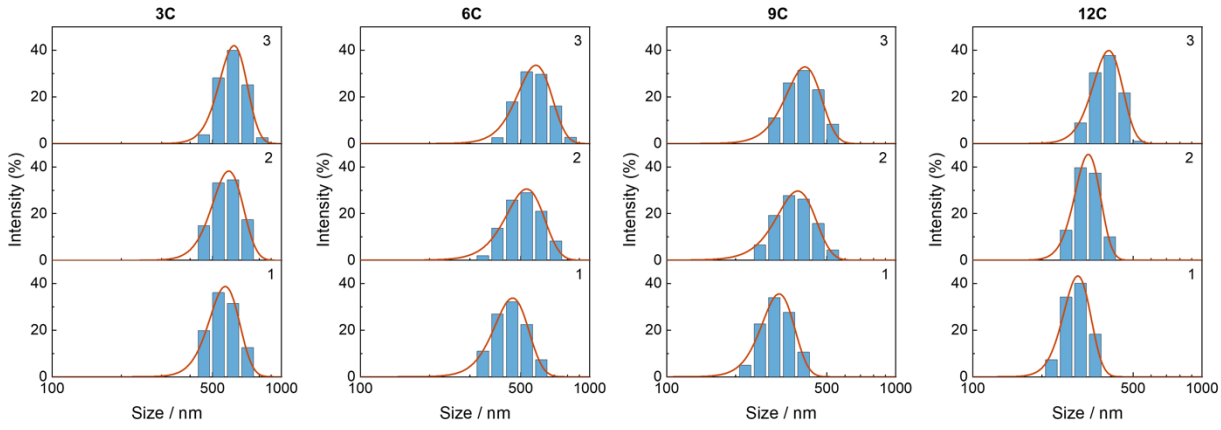

Figure S7. The particle size distribution of the COF samples after 0.06 h with different amounts of competitors, determined via the DLS method. The solid red lines indicate a fit to the normal distribution.

S8. Sufficiency of the KMC Box Size

We tested the effect of the box size chosen for the KMC simulations on the obtained yield results. The breadth and width of the box were both increased twofold, leading the lateral area

of the box to increase by four times. The resultant yield curves for the 0C, 3C, 6C, 9C and 12C cases seen in Figure S8 indicate that there are no significant deviations from the yield curves obtained with the box size used in the main text, i.e., a 50 × 50 lattice for the 2D COF.

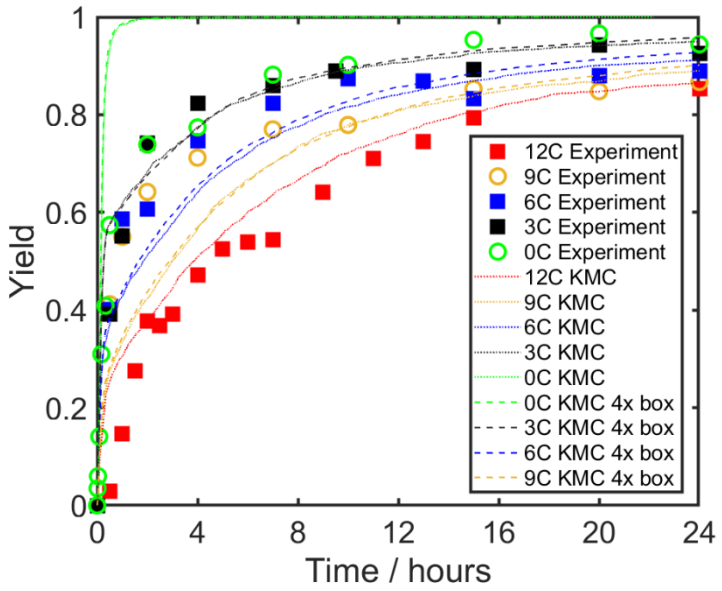

Figure S8. COF yield obtained from the KMC simulations, as a function of time, for different amounts of inhibitors in the system. The symbols represent the experimental data and dotted lines represent the KMC predictions. The dashed lines represent the KMC predictions with an increased box size. Note that the yield is dimensionless.